Received: 23 October 2023 | Accepted: 18 February 2024

DOI: 10.1002/eer2.73

RESEARCH ARTICLE

Earthquake Engineering and Resilience WILEY

Nonresilience curve: A new tool for use in resilience assessment

Cao Wang

School of Civil, Mining, Environmental and Architectural Engineering, University of Wollongong, Wollongong, NSW, Australia

Correspondence
Cao Wang, School of Civil, Mining, Environmental and Architectural Engineering, University of Wollongong, Room 130, Bldg 4, Wollongong, NSW 2522, Australia.
Email: wangc@uow.edu.au

Funding information
University of Wollongong; Career Development Fellowship; Vice-Chancellor's Postdoctoral Research Fellowship

Abstract

Resilience assessment is a widely used method to evaluate the ability of an object (e.g., an individual structure, or a system consisting of multiple interacting structures) to withstand, recover from, and adapt to disruptive events. This paper proposes a novel concept of "nonresilience curve," which measures the nonresilience (complement of resilience) of an object of interest conditional on a specific hazard intensity. It is by nature an extension of the well-established fragility curves, integrating the multiple damage states of a posthazard object. The applicability of the proposed nonresilience curve to individual structures and systems (including series systems, parallel systems, and more general and complicated systems) has been demonstrated in this paper. It is also preliminarily shown that the shape of the cumulative distribution function of a lognormal distribution is suitable to approximate the nonresilience curve, if only limited data points associated with the target nonresilience curve are available. Since the nonresilience curve is a function of the hazard intensity measure (IM), one can estimate the nonresilience of an object in a fully probabilistic manner by additionally taking into account the uncertainty associated with the IM. The proposed nonresilience curve can be further extended to formulate nonresilience surface, which is a joint function of both the IM and the available resource that supports the posthazard recovery process. The nonresilience curve is promising to be adopted in engineering practice for resilience assessment and resilience-based design of civil structures and infrastructure systems.

KEYWORDS

fragility curve, nonresilience curve, nonresilience surface, resilience, system nonresilience

1 | INTRODUCTION

Resilience of an object (e.g., an individual structure, a system consisting of multiple interacting facilities, or a community) refers to the ability to return to the original state in the aftermath of disruptive events (e.g., natural hazards).[1–5] Supposing that a hazardous event occurs at time t_0, the resilience can be measured by the integrated

performance function of an object from t_0 to a reference time. For example, Bruneau et al.[1] defined the resilience loss as $\int_{t_0}^{t_1}[1-Q(t)]\,dt$ over a time domain of $[t_0, t_1]$, where $Q(t)$ is the performance/functionality of an object at time t (varying between 0 and 1), and t_1 is the time of full recovery. Further, a dimensionless resilience model, denoted by R_e, is as follows[6–8]:

$$R_e = \frac{1}{t_h - t_0}\int_{t_0}^{t_h} Q(t)\,dt \tag{1}$$

where t_h is the reference time (e.g., it may refer to the time of full recovery[9,10]). The resilience model in Equation (1) has been widely utilized in the literature to measure the resilience of objects at different scales.[11–16] A generalized form of Equation (1) was proposed by Wang[17] to reflect the sensitivity of resilience to the variation of functionality, which is expressed as follows:

$$R_e = f^{-1}\left(\frac{1}{t_h - t_0}\int_{t_0}^{t_h} f\left[Q(t)\right]dt\right) \tag{2}$$

where $f(x)$ is a generating function, which allows the asset owners/decision makers to select a personalized resilience model that reflects their attitude towards the extremely low serviceability of an object. It is a monotonic function of $x \in [0, 1]$, with which R_e in Equation (2) varies within $[0, 1]$ based on the mean value theorem for integrals.[17] For example, if selecting $f(x) = x$, then Equation (2) reduces to Equation (1), where the resilience is determined by the arithmetic mean of the performance function over $[t_0, t_h]$. On the other hand, if assigning $f(x) = \ln x$, then the resilience over $[t_0, t_h]$ is more sensitive to the extremely small value of $Q(t)$, because it has been evaluated based on the geometric mean of the performance function. In this paper, the resilience model in Equation (2) will be used, along with the following two generating functions: $f_1(x) = x$, and $f_2(x) = \ln x$. In some occasions it is more convenient to use the term "nonresilience," which equals 1 minus resilience.

The resilience depends on the load-resisting capacity of the object, the intensity measure (IM) of a hazardous event, and the available resource that supports the posthazard recovery process (affecting the recovery expeditiousness). As a result, resilience assessment of an object could be computationally costly in the presence of many influencing factors. With this regard, simple analytical tools, if present, would be beneficial to improve the efficiency of resilience evaluation. A relevant example is that, in terms of performance assessment of civil structures and infrastructure systems, fragility curves have been widely employed in engineering practice to model the posthazard damage states (DSs), evaluating the occurrence probability of a particular DS conditional on the hazard IM.[18–21] Let $\mathcal{F}(x)$ be a fragility function of $IM = x$ (its graph is known as fragility curve). One can efficiently evaluate the occurrence probability of a DS caused by a hazardous event in a fully probabilistic manner by taking into account the uncertainty associated with the IM and the fragility model. Denote $f_{IM}(x)$ the probability distribution function (PDF) of the IM, the probability of a DS related to $\mathcal{F}(x)$, $\Pr(DS)$, is evaluated as follows using the law of total probability:

$$\Pr(DS) = \int_0^{\infty} \mathcal{F}(x) f_{IM}(x)\,dx \tag{3}$$

in which Pr() denotes the probability of the event in the brackets.

Motivated by Equation (3), if there exists such a function $\mathcal{N}(x)$, which returns the nonresilience of an object of interest conditional on $IM = x$, then the nonresilience can be evaluated as follows in a convenient way:

$$\text{Nonresilience} = \int_0^{\infty} \mathcal{N}(x) f_{IM}(x)\,dx \tag{4}$$

In Equation (4), one can interpret $\mathcal{N}(x)$ as the nonresilience conditional on the IM being x. As such, the many factors that affect the nonresilience of an object (e.g., available resource that supports the posthazard recovery, the hazard-resisting capacity, and others), as well as the uncertainties associated with these factors, have been collectively assembled in the function $\mathcal{N}(x)$. This is similar to the fragility curve $\mathcal{F}(x)$ in Equation (3), which has incorporated the affecting factors on the formulation of DSs except the hazard IM.[22]

The aim of this paper is to develop the function $\mathcal{N}(t)$ for various objects including individual structures and different types of systems. This is deemed as an effective approach to improving the efficiency of resilience assessment. The graph of $\mathcal{N}(t)$ is named "nonresilience curve"—a novel concept proposed in this paper—which measures the nonresilience of an object conditional on a specific IM of a hazardous event. The nonresilience curve can thus enable the resilience of an object of interest to be conveniently evaluated in a fully probabilistic manner given the PDF of IM, as revealed in Equation (4). This paper will discuss the applicability of the nonresilience curve to individual structures and systems consisting of multiple interacting components (including series systems, parallel systems, and more general systems). Sensitivity analyses will also be conducted to investigate the role of affecting factors (e.g., available resources, topology of the system, and correlation between components) in the nonresilience curve.

2 | NONRESILIENCE CURVE OF AN INDIVIDUAL STRUCTURE

In this section, the nonresilience curve of an individual structure is discussed, which is built based on the fragility curves that represent multiple DSs of a posthazard structure.

A fragility curve is typically assumed to have a lognormal distribution shape.[22] Thus, one can interpret the fragility curve as the cumulative distribution function (CDF) of a lognormal variable R^*, named "generalized capacity."[23–25] The PDF of R^*, $f_{R^*}(r)$, takes a form of

$$f_{R^*}(x) = \frac{1}{\sqrt{2\pi}x\nu}\exp\left[-\frac{1}{2}\left(\frac{\ln x - \kappa}{\nu}\right)^2\right], \quad x \geq 0 \tag{5}$$

where κ and ν are the mean value and the standard deviation of $\ln R^*$, respectively, and satisfy

$$\mu_{R^*} = \exp(\kappa + 0.5\nu^2), \quad \sigma^2_{R^*} = \mu^2_{R^*}[\exp(\nu^2) - 1] \tag{6}$$

in which μ_{R^*} and $\sigma^2_{R^*}$ are the mean value and the variance of R, respectively.

In the aftermath of a hazardous event, a structure may suffer from one of the multiple DSs, for example, slight damage, moderate damage, among others.[26,27] This corresponds to multiple generalized capacities, denoted by $R^*_1, R^*_2, ..., R^*_m$ in the presence of m fragility curves (and thus $m + 1$ DSs). It was shown in Wang et al.[24] that each generalized capacity is statistically fully correlated so as to match the definition of fragility curves. Let $F_{R^*_j}(x)$ be the CDF of R^*_j (i.e., the jth fragility curve) for $j = 1, 2, ..., m$. Wang et al.[28] proposed a concept of "resilience capacity" for individual structures, written as $\widetilde{R}$, which is a generalized form of the generalized capacity.

In this paper, the nonresilience function $\mathcal{N}(x)$ is interpreted as the CDF of $\widetilde{R}$, which is comparable to the fact that the fragility curve is the CDF of a generalized capacity. With this, Figure 1 illustrates the relationship between the following four items: generalized capacity, resilience capacity, fragility curve, and nonresilience curve.

Mathematically, the nonresilience function $\mathcal{N}(x)$ is equal to the CDF of $\widetilde{R}$, $F_{\widetilde{R}}(x)$, and is expressed as follows according to Wang et al.[28]:

$$\mathcal{N}(x) = F_{\widetilde{R}}(x) = 1 - \sum_{j=0}^{m} \overline{R}_{e,j} \cdot p_j(x) \tag{7}$$

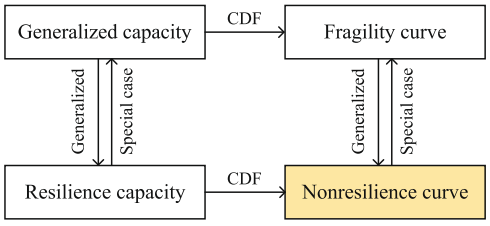

FIGURE 1 Relationship between four quantities. The highlighted "nonresilience curve" is a novel concept proposed in this paper. CDF, cumulative distribution function.

in which $\overline{R}_{e,j}$ is the mean value of resilience conditional on the occurrence of the jth DS (totally $m+1$ DSs are considered), having a value within [0, 1], and $p_j(x)$ is the occurrence probability of the jth DS, which is evaluated according to

$$p_j(x) = F_{R_j^*}(x) - F_{R_{j+1}^*}(x), \quad j = 0, 1, ..., m \tag{8}$$

where $R_0^* \equiv 0$, and $R_{m+1}^* \equiv \infty$ are two auxiliary generalized capacities. The 0th DS means "no damage." Note that each $\overline{R}_{e,j}$ in Equation (7) varies within [0, 1], and $\sum_{j=0}^{m} p_j(x) = 1$, with which $\mathcal{N}(x) \in [0, 1]$. This is consistent with the definition of a CDF. Further, conditional on $IM = x$, the mean value of resilience equals $1 - \mathcal{N}(x)$ based on Equation (7).

Equation (7) shows that nonresilience function $\mathcal{N}(x)$ is built based on the fragility curves (see the item $F_{R_j^*}(x)$). Figure 2 illustrates the comparison and connection between nonresilience curve and fragility curve for a specific case of $m = 4$ (this can be naturally extended to the case with other number of fragility curves). Totally $m + 1 = 5$ DSs are thus involved, denoted by $DS0$ through to $DS4$, respectively ($DS0$ = no damage). Conditional on $IM = x$, the occurrence probability of DSj is p_j for $j = 0, 1, ..., m$, as shown in Figure 2A. The remaining functionality of the structure due to the occurrence of a hazardous event, q_r, is dependent on the DS. Using the resilience model in Equation (2), one can compute $\overline{R}_{e,j}$ for each DSj. Finally, the nonresilience function $\mathcal{N}(x)$ is obtained as $1 - \mathbf{R}_e \cdot \mathbf{p}$, where $\mathbf{R}_e = [\overline{R}_{e,0}, \overline{R}_{e,1}, \overline{R}_{e,2}, ..., \overline{R}_{e,m}]$, and $\mathbf{p} = [p_0, p_1, ..., p_m]$.

The proposed nonresilience curve, as illustrated in Figure 2C, focuses on the "nonresilience" of an object (e.g., an individual structure), and thus has a similar trend to a fragility curve as a function of IM (i.e., with a greater hazard intensity, the object is more "fragile" and thus is less "resilient"). Note also that the term "resilience curve" has been used in some previous studies[29,30] to represent the change of performance over time (under this context, one example is shown in Figure 2B), which has different significance compared with the proposed nonresilience curve in this paper, and thus should be used with carefulness. The advantage of the latter (proposed nonresilience curve) is that it yields the conditional nonresilience on IM by collectively integrating the affecting factors on resilience over the time domain.

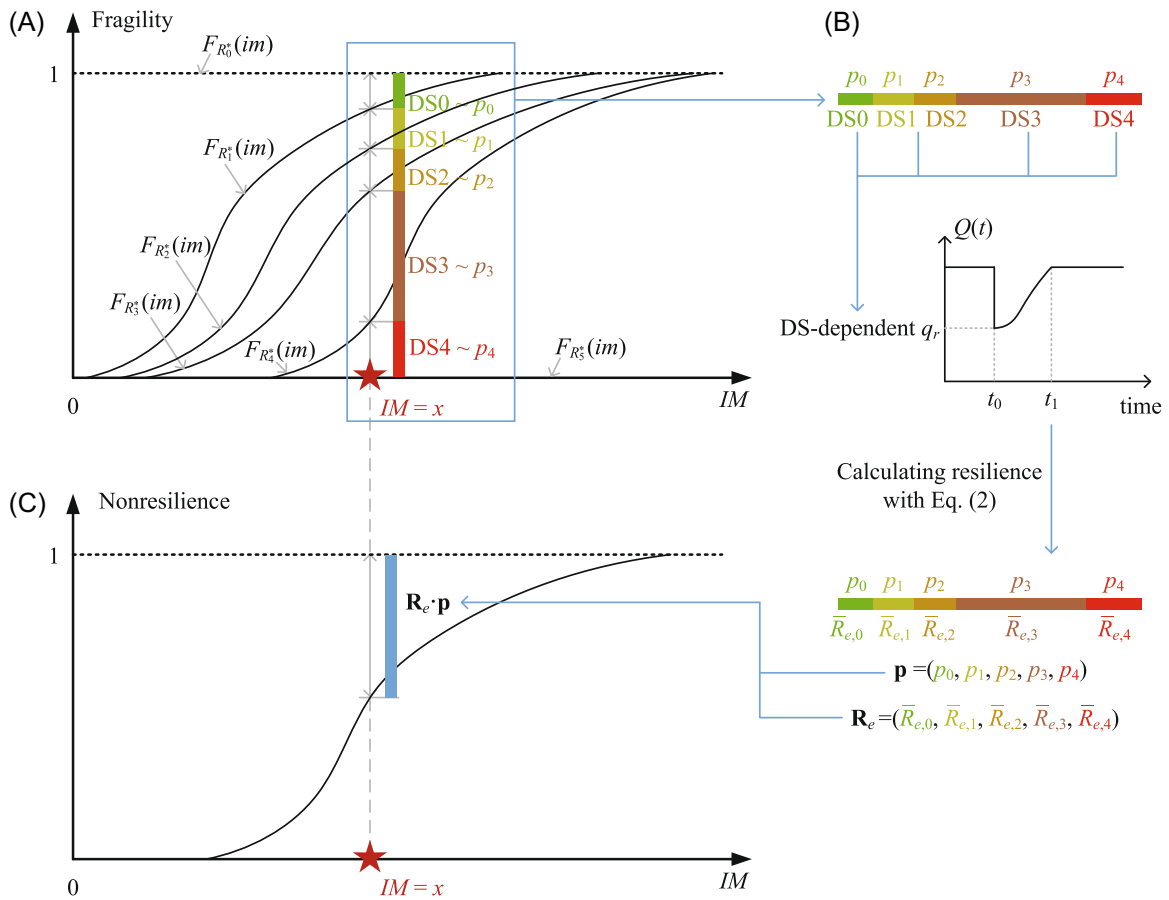

FIGURE 2 Formulation of nonresilience curve based on fragility curves. (A) Fragility curve, (B) steps to establish nonresilience curve, and (C) nonresilience curve.

Next, the item $\overline{R}_{e,j}$ in Equation (7) is derived based on the resilience model in Equation (2). As illustrated in Figure 3, a hazardous event occurs at time t_0, with which the performance function $Q(t)$ decreases from 1 to q_r linearly until time $t_0 + \Delta_f$. The changing rate of $Q(t)$ is thus equal to $K_f = -(1 - q_r)/\Delta_f$ during $[t_0, t_0 + \Delta_f]$. This is followed by a recovery process with a duration of Δ. It is assumed that $Q(t)$ equals q_r during the recovery process and becomes 1 (the pre-hazard state) upon completion of recovery. This is consistent with the recommendation by Ayyub[31] unless sufficient data are collected and classifications are made to justify other recovery models. A reference period of $[t_0, t_h] = [t_0, t_0 + \Delta_{\text{ref}}]$ is considered. The item Δ_{ref} is also known as "control time" in some previous studies,[6,13] which is usually decided by the asset owner/decision maker.

Denote $\Delta_d = \Delta_{ref} - \Delta_f$. The recovery time Δ is dependent on both q_r and the available resource $\mathcal{R}$, and is expressed by a function ζ as follows: $\Delta = \zeta(\mathcal{R}, q_r)$. Define $\Omega_1 = \{q : \zeta(\mathcal{R}, q) < \Delta_{\text{d}} \cap 0 \le q \le 1\}$, and $\Omega_2 = \{q : \zeta(\mathcal{R}, q) \ge \Delta_{\text{d}} \cap 0 \le q \le 1\}$. If $q_r \in \Omega_1$, then the recovery process is completed before t_h, as shown in Figure 3A. On the other hand, if $q_r \in \Omega_2$, then the recovery is still in progress until time t_h, as illustrated in Figure 3B.

Corresponding to the jth DS, let $f_{Q_{r,j}}(q)$ be the PDF of the posthazard remaining functionality. One can derive $\overline{R}_{e,j}$ by considering the two cases in Figure 3 and using the law of total probability (note the occurrence probability of case (A) equals $\int_{\Omega_1} f_{Q_{r,j}}(q)\,dq$, and that associated with case (B) is $\int_{\Omega_2} f_{Q_{r,j}}(q)\,dq$. On the basis of Equation (2), if the generating function is $f_1(x) = x$, it follows that

$$\begin{aligned}
\overline{R}_{e,j} &= \frac{1}{\Delta_{\text{ref}}} \int_{\Omega_1} \left\{ \int_{t_0}^{t_0+\Delta_{\text{f}}} [K_{\text{f}}(t - t_0 - \Delta_{\text{f}}) + q]\,dt + q\Delta + (\Delta_{\text{d}} - \Delta) \right\} f_{Q_{r,j}}(q)\,dq \\
&\quad + \frac{1}{\Delta_{\text{ref}}} \int_{\Omega_2} \left\{ \int_{t_0}^{t_0+\Delta_{\text{f}}} [K_{\text{f}}(t - t_0 - \Delta_{\text{f}}) + q]\,dt + q\Delta_{\text{d}} \right\} f_{Q_{r,j}}(q)\,dq \\
&= \int_{\Omega_1} \frac{1}{\Delta_{\text{ref}}} \left(\frac{1}{2}\Delta_{\text{f}} + \frac{1}{2} q\Delta_{\text{f}} + \Delta_{\text{d}} + (q-1)\zeta(\mathcal{R}, q) \right) f_{Q_{r,j}}(q)\,dq \\
&\quad + \int_{\Omega_2} \frac{1}{\Delta_{\text{ref}}} \left(\frac{1}{2}\Delta_{\text{f}} + \frac{1}{2} q\Delta_{\text{f}} + q\Delta_{\text{d}} \right) f_{Q_{r,j}}(q)\,dq
\end{aligned} \tag{9}$$

Similarly, with $f_2(x) = \ln x$, one has

$$\begin{aligned}
\overline{R}_{e,j} &= \int_{\Omega_1} \exp\left\{ \frac{1}{\Delta_{\text{ref}}} \int_{t_0}^{t_0+\Delta_{\text{f}}} \ln[K_{\text{f}}(t - t_0 - \Delta_{\text{f}}) + q]\,dt + \frac{\Delta}{\Delta_{\text{ref}}} \ln q \right\} f_{Q_{r,j}}(q)\,dq \\
&\quad + \int_{\Omega_2} \exp\left\{ \frac{1}{\Delta_{\text{ref}}} \int_{t_0}^{t_0+\Delta_{\text{f}}} \ln[K_{\text{f}}(t - t_0 - \Delta_{\text{f}}) + q]\,dt + \frac{\Delta_{\text{d}}}{\Delta_{\text{ref}}} \ln q \right\} f_{Q_{r,j}}(q)\,dq \\
&= \int_{\Omega_1} \exp\left\{ -\frac{1}{\Delta_{\text{ref}}} \cdot \left[\left(1 + \frac{q \ln q}{1-q} \right) \Delta_{\text{f}} - \zeta(\mathcal{R}, q) \ln q \right] \right\} f_{Q_{r,j}}(q)\,dq \\
&\quad + \int_{\Omega_2} \exp\left\{ -\frac{1}{\Delta_{\text{ref}}} \cdot \left[\left(1 + \frac{q \ln q}{1-q} \right) \Delta_{\text{f}} - \Delta_{\text{d}} \ln q \right] \right\} f_{Q_{r,j}}(q)\,dq
\end{aligned} \tag{10}$$

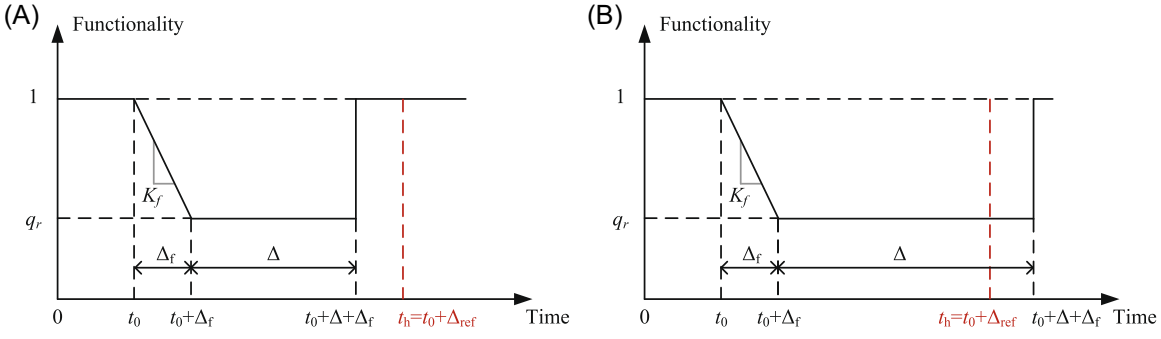

FIGURE 3 Time-variation of performance $Q(t)$ associated with a hazard occurring at time t_0. (A) $\Delta \le \Delta_d$, and (B) $\Delta > \Delta_d$.

Substituting Equations (9) and (10) into Equation (7), one can obtain the nonresilience function $\mathcal{N}(x)$ (and thus the nonresilience curve) in an explicit form.

Note that in Equation (4), the IM, having a PDF of $f_{IM}(x)$, has been associated with a single hazardous event, yielding the evaluation of nonresilience due to the occurrence of one event. For a time interval $\mathscr{D}$ within which the occurrence of hazards follows a Poisson process with an occurrence rate of λ, let $f_{IM,\mathscr{D}}(x)$ be the PDF associated with the maximum IM of all the hazardous events over the time domain $\mathscr{D}$. One can replace the item $f_{IM}(x)$ in Equation (4) with $f_{IM,\mathscr{D}}(x)$ to compute the resilience due to the maximum IM over $\mathscr{D}$, denoted by Nonresilience($\mathscr{D}$). This point is explained as follows.

On the basis of Equation (4), using the law of total probability, it follows that

$$\text{Nonresilience}(\mathscr{D}) = \sum_{i=0}^{\infty}\left[\Pr(\text{occurrence of } i \text{ event(s)}) \cdot \int_0^{\infty} \mathcal{N}(x) f_{IM,i}(x)\,dx\right] \tag{11}$$

in which $f_{IM,i}$ is the PDF of the maximum IM over $\mathscr{D}$ conditional on the occurrence of i hazardous event(s). Following the property of a Poisson process,[32] one has

$$\Pr(\text{occurrence of } i \text{ event(s)}) = \frac{(\lambda\mathscr{D})^i}{i!}\exp(-\lambda\mathscr{D}), \quad i = 0, 1, 2, \ldots \tag{12}$$

Let $F_{IM}(x)$ be the CDF of IM associated with a single hazardous event ($f_{IM}(x) = dF_{IM}(x)/dx$), $F_{IM,i}(x)$ the CDF of the maximum IM over $\mathscr{D}$ conditional on the occurrence of i hazardous event(s) ($F_{IM,i}(x) = F_{IM}^i(x)$ for $i = 0, 1, 2, \ldots$), and $F_{IM,\mathscr{D}}$ the CDF of the maximum IM of all the hazardous events over $\mathscr{D}$ ($f_{IM,\mathscr{D}}(x) = dF_{IM,\mathscr{D}}(x)/dx$). On the basis of Equation (12), it follows that

$$F_{IM,\mathscr{D}}(x) = \sum_{i=0}^{\infty}\frac{(\lambda\mathscr{D})^i}{i!}\exp(-\lambda\mathscr{D}) \cdot F_{IM,i}(x) = \exp[-\lambda\mathscr{D}(1 - F_{IM}(x))] \tag{13}$$

Further, with Equation (12), Equation (11) becomes

$$\text{Nonresilience}(\mathscr{D}) = \int_0^{\infty} \mathcal{N}(x) h_{\mathscr{D}}(x)\,dx \tag{14}$$

where

$$\begin{aligned} h_{\mathscr{D}}(x) &= \sum_{i=0}^{\infty}\frac{(\lambda\mathscr{D})^i}{i!}\exp(-\lambda\mathscr{D}) \cdot f_{IM,i}(x) = \sum_{i=0}^{\infty}\frac{(\lambda\mathscr{D})^i}{i!}\exp(-\lambda\mathscr{D}) \cdot i \cdot F_{IM}^{i-1}(x) \cdot f_{IM}(x) \\ &= \sum_{i=1}^{\infty}\left[\frac{(F_{IM}(x) \cdot \lambda\mathscr{D})^{i-1}}{(i-1)!}\exp(-\lambda\mathscr{D})\cdot\right] \cdot \lambda\mathscr{D} f_{IM}(x) = \exp(\lambda\mathscr{D}F_{IM}(x)) \cdot \exp(-\lambda\mathscr{D}) \cdot \lambda\mathscr{D} f_{IM}(x) \\ &= f_{IM,\mathscr{D}}(x) \end{aligned} \tag{15}$$

Equation (14) demonstrates that the resilience due to the maximum IM over $\mathscr{D}$ can be evaluated by simply replacing the PDF of IM in Equation (4) with $f_{IM,\mathscr{D}}(x)$.

3 | NONRESILIENCE CURVE OF A SERIES SYSTEM

In this section, the nonresilience curve associated with a series system is discussed. A series system consisting of n components is defined herein as such a configuration that the system functionality equals the minimum of all the functionalities associated with the components. For example, if any of the components fails with a zero functionality, then the system functionality also degrades to zero.

The construction of the nonresilience function $\mathcal{N}(x)$ for a series system follows a similar concept as that for an individual structure (component); however, additional considerations include: (1) the modeling of correlation between

the generalized capacities associated with different components, and (2) optimal resource allocation strategy that supports the recovery of system functionality.

For (1), note that a correlation between component performances may arise due to common construction practices and design codes.[33] In this paper, such correlation is reflected through a correlated sequence $\mathbf{R}_1^* = [R_{1,1}^*, R_{2,1}^*, ..., R_{n,1}^*]$, where $R_{i,1}^*$ is the generalized capacity associated with the ith component and $DS1$ (as mentioned above, for each individual component, its multiple generalized capacities are fully correlated[24]). To this end, one can use the Nataf transformation method to generate a sample for $\mathbf{R}_1^*$. The technical details have been well documented in the literature,[34–36] and are summarized briefly herein.

With the fragility curves for each component, the marginal distribution of $\mathbf{R}_1^*$ is known. Let $\boldsymbol{\rho} = [\rho_{ij}]$ be the correlation matrix of $\mathbf{R}_1^*$ (i.e., ρ_{ij} is the correlation coefficient between $R_{i,1}^*$ and $R_{j,1}^*$). First, $\mathbf{R}_1^*$ is transformed to a correlated standard normal vector $\mathbf{Y} = \{Y_1, Y_2, ..., Y_n\}$ with a correlation matrix of $\boldsymbol{\rho}' = [\rho_{ij}']$ according to $F_{R_{i,1}^*}(R_{i,1}^*) = \Phi(Y_i)$, where $F_{R_{i,1}^*}()$ is the CDF of $R_{i,1}^*$. Next, $\mathbf{Y}$ is mapped to an independent standard normal vector $\mathbf{Z} = \{Z_1, Z_2, ..., Z_n\}$ by $\mathbf{Y} = \mathbf{L} \cdot \mathbf{Z}$, where $\mathbf{L} = [l_{ij}]$ is a lower triangle matrix satisfying $\mathbf{L} \cdot \mathbf{L}^\top = \boldsymbol{\rho}'$ (the symbol $\top$ means transpose of matrix). It is a relatively simple task to generate a sample for $\mathbf{Z}$, denoted by $\mathbf{z}$. With this, one can find $\mathbf{y} = \mathbf{L} \cdot \mathbf{z}$, and then $\mathbf{r}_1^* = [r_{1,1}^*, r_{2,1}^*, ..., r_{n,1}^*]$ (a sample of $\mathbf{R}_1^*$) according to $r_{i,1}^* = F_{R_{i,1}^*}^{-1}[\Phi(y_i)]$, $i = 1, 2, ..., n$.

Another important feature of the system nonresilience curve, compared with that for an individual structure, is that there may be multiple damaged components in the aftermath of a hazardous event, and thus one needs to find the optimal resource allocation strategy to ensure that the system functionality is restored with expeditiousness. The recovery process is dependent on "how the system has been damaged," that is, the sequence of remaining functionalities $q_{r,1}, q_{r,2}, ..., q_{r,n}$, in which $q_{r,i}$ is the remaining functionality associated with the ith component immediately before the recovery process, $i = 1, 2, ..., n$. The reduced system functionality due to a hazardous event, q_{sys} is determined by $q_{\text{sys}} = \min(q_{r,1}, q_{r,2}, ..., q_{r,n})$ by definition.

The system resilience problem is illustrated in Figure 4. Due to a hazardous event occurring at time t_0, the system's remaining functionality degrades from 1 to q_{sys} until time $t_0 + \Delta_{\text{f}}$. This is followed by a recovery process with a duration of Δ_{sys}. The system resilience is evaluated by considering the performance function over $[t_0, t_h] = [t_0, t_0 + \Delta_{\text{ref}}]$.

Due to the hazardous event, if any of the components fails/collapses with a remaining functionality being zero, then $q_{\text{sys}} = \min(q_{r,1}, q_{r,2}, ..., q_{r,n}) = 0$, indicating that the system also fails. This corresponds to a zero resilience for the system, which can be achieved through using the resilience model in Equation (2) with $f_2(x)$ despite the value of Δ_{f}, as observed from Figure 6. If all components are in the state of "no damage," then $q_{\text{sys}} = 1$, leading to the system resilience being 1. For more general cases where $0 < q_{\text{sys}} < 1$, the optimal resource allocation is determined by $\min \max(\Delta_1, \Delta_2, ..., \Delta_n)$, in which Δ_i is the duration of the recovery process associated with the ith component ($i = 1, 2, ..., n$). Let $\mathcal{R}$ be the total resource, and $\mathcal{R}_i$ the resource allocated to the ith component. It follows that $\sum_{i=1}^{n} \mathcal{R}_i = \mathcal{R}$. The recovery time Δ_i is affected by both $q_{r,i}$ and $\mathcal{R}_i$, and is expressed by a function ζ_i as follows: $\Delta_i = \zeta_i(\mathcal{R}_i, q_{r,i})$. In particular, with a fixed $q_{r,i}$, $\zeta_i(\mathcal{R}_i, q_{r,i})$ is rewritten as $\zeta_i(\mathcal{R}_i)$ for simplicity. Without loss of generality, assume that $\zeta_i(\mathcal{R}_i)$ is a monotonically decreasing function of $\mathcal{R}_i$ (i.e., greater amount of resource results in a smaller recovery duration).

Denote $\Delta_j = \max(\Delta_1, \Delta_2, ..., \Delta_n)$, that is,

$$\zeta_j(\mathcal{R}_j) \geq \zeta_i(\mathcal{R}_i), \qquad \forall i = 1, 2, ..., n \tag{16}$$

Or equivalently,

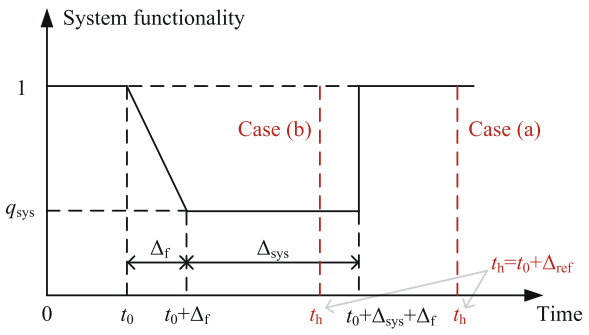

FIGURE 4 Illustration of system functionality and system resilience.

$$\zeta_i^{-1}[\zeta_j(\mathcal{R}_j)] \le \mathcal{R}_i, \qquad \forall i = 1, 2, ..., n \tag{17}$$

On the basis of Equation (17), a sequence of nonnegative variables $\epsilon_1, \epsilon_2, ..., \epsilon_n$ is introduced, which satisfies

$$\mathcal{R}_i = \epsilon_i + \zeta_i^{-1}[\zeta_j(\mathcal{R}_j)], \qquad \forall i = 1, 2, ..., n \tag{18}$$

Thus,

$$\sum_{i=1}^{n} \mathcal{R}_i = \sum_{i=1}^{n} \epsilon_i + \sum_{i=1}^{n} \zeta_i^{-1}[\zeta_j(\mathcal{R}_j)] = \mathcal{R} \tag{19}$$

Recall that the optimization problem herein is min $\zeta_j(\mathcal{R}_j)$. Introduce a function $g(x) = \sum_{i=1}^{n} \zeta_i^{-1}(x)$. Note that $g(x)$ is a monotonically decreasing function of x (because each $\zeta_i^{-1}(x)$ is a decreasing function of x), and that $g(0) = \infty, g(\infty) = 0$. This guarantees the existence of a unique root of $g(x) = \mathcal{R}$, denoted by x_0. With this, one has

$$g[\zeta_j(\mathcal{R}_j)] = \mathcal{R} - \sum_{i=1}^{n} \epsilon_i \le \mathcal{R} = g(x_0) \tag{20}$$

Thus, $\zeta_j(\mathcal{R}_j) \ge x_0$ due to the monotonicity of $g(x)$. The equality holds when $\epsilon_i = 0$ for $\forall i = 1, 2, ..., n$. This corresponds to each $\mathcal{R}_i$ expressed as follows:

$$\mathcal{R}_i = \zeta_i^{-1}(x_0), \qquad \forall i = 1, 2, ..., n \tag{21}$$

Equation (21) gives the optimal solution to the resource allocation that minimizes the duration of system recovery. On the basis of Equation (21), the recovery duration associated with each component, Δ_i, identically equal to x_0. This further leads to $\Delta_{\text{sys}} = x_0$.

Now, with q_{sys} and Δ_{sys} ready, the system resilience can be calculated by referring to Figure 4. For case (A) with $\Delta_{\text{d}} > \Delta_{\text{sys}}$, a sample resilience, $R_{e,\text{sample}}$, is computed as follows (the subscript "sample" is used because the resilience is conditional on the sequence of remaining functionalities $q_{r,1}, q_{r,2}, ..., q_{r,n}$), which is based on the resilience model in Equation (2) with $f_2(x)$.

$$R_{e,\text{sample}} = \exp\left\{-\frac{1}{\Delta_{\text{ref}}}\left[\Delta_{\text{f}} + \frac{q_{\text{sys}}\Delta_{\text{f}} \ln q_{\text{sys}}}{1 - q_{\text{sys}}} - \Delta_{\text{sys}} \ln q_{\text{sys}}\right]\right\} \tag{22}$$

Similarly, for case (B) in Figure 4,

$$R_{e,\text{sample}} = \exp\left\{-\frac{1}{\Delta_{\text{ref}}}\left[\Delta_{\text{f}} + \frac{q_{\text{sys}}\Delta_{\text{f}} \ln q_{\text{sys}}}{1 - q_{\text{sys}}} - \Delta_{d} \ln q_{\text{sys}}\right]\right\} \tag{23}$$

Conditional on a specific $IM = x$, one can use the Monte Carlo simulation to generate the nonresilience curve. Basically, for the ℓth simulation run ($\ell = 1, 2, ...$), a sequence of $q_{r,1}, q_{r,2}, ..., q_{r,n}$ is sampled first, and a sample value of nonresilience is obtained through Equation (22) or (23), denoted by $R_{e,\text{sample},\ell}$. With totally M replications of simulation, $\mathcal{N}(x)$ is approximated by $\sum_{\ell=1}^{M} R_{e,\text{sample},\ell}$, which is guaranteed by the strong law of large numbers.

4 | NONRESILIENCE CURVE OF A PARALLEL SYSTEM

The nonresilience curve of a parallel system is discussed in this section. A parallel system consisting of n components has the property that the system functionality equals the maximum of the functionalities associated with all the components. Due to the similarity between the definitions of series and parallel systems, the establishment of

nonresilience function $\mathcal{N}(x)$ for a parallel is similar to the case of a series system, including the modeling of component correlation. The difference, however, is on the determination of q_{sys} and Δ_{sys}. The symbols and notations for series systems will be adopted herein, unless otherwise stated.

On the basis of the definition of a parallel system, $q_{\text{sys}} = \max(q_{r,1}, q_{r,2}, ..., q_{r,n})$. If all the components fail/collapse with remaining functionalities being zero, then $q_{\text{sys}} = \max(q_{r,1}, q_{r,2}, ..., q_{r,n}) = 0$, with which the system also fails and has zero resilience. If at least one of the components is in the state of "no damage," having a remaining functionality of 1, then $q_{\text{sys}} = 1$, yielding the system resilience being 1. For more general cases where $0 < q_{\text{sys}} < 1$, one would need to seek for the optimal resource allocation strategy. As illustrated in Figure 4, the target is to minimize the recovery duration for the system. This is expressed, mathematically, as follows: $\min \min(\Delta_1, \Delta_2, ..., \Delta_n)$, where $\Delta_i = \zeta_i(\mathcal{R}_i)$ as before (written in such a way as it is conditional on $q_{r,i}$).

Denote $\zeta_j(\mathcal{R}) = \min \zeta_i(\mathcal{R})$, that is, the jth component suffers from the least damage and can be restored the most rapidly in the presence of the same resource. Note that

$$\zeta_i(\mathcal{R}_i) \geq \zeta_i(\mathcal{R}) \quad \text{for } \forall i = 1, 2, ..., n \tag{24}$$

and thus,

$$\min \zeta_i(\mathcal{R}_i) \geq \min \zeta_i(\mathcal{R}) = \zeta_j(\mathcal{R}) \tag{25}$$

Equation (25) indicates that the minimum of $\min(\Delta_1, \Delta_2, ..., \Delta_n)$ is achieved by $\zeta_j(\mathcal{R})$, that is, the optimal resource allocation strategy is to repair the jth component (suffering from the least damage) with full resource. As a result, it follows that $\Delta_{\text{sys}} = \zeta_j(\mathcal{R})$. Now, with q_{sys} and Δ_{sys} obtained conditional on a sequence $q_{r,1}, q_{r,2}, ..., q_{r,n}$, a sample value of resilience can be computed using Equation (22) or (23). This completes the steps for generating the nonresilience function based on Monte Carlo simulation.

5 | NONRESILIENCE CURVE OF A GENERAL SYSTEM

In many engineering applications, a system cannot be simply categorized as either a series or a parallel system; rather, it may have a more complicated topology. For illustration purpose, this section will focus on a specific example of the general system, as shown in Figure 5A, addressing the construction of its nonresilience curve. The symbols and notations for series systems will be adopted herein.

The establishment of nonresilience curve for the seven-component system in Figure 5A follows the steps for that of a series system with modification. The feature of the general system linking points A and B, compared with a series system, is the dependence of both q_{sys} and Δ_{sys} on the system topology. The system's posthazard functionality is determined by $q_{\text{sys}} = \min(q_{r,1}, \max(q_{r,2}, q_{r,3}, q_{r,4}), q_{r,5}, \max(q_{r,6}, q_{r,7}))$. Further, if $0 < q_{\text{sys}} < 1$, by referring to Figure 4, the optimal resource allocation strategy is to minimize the recovery duration for the system, which is mathematically expressed as $\min \max(\Delta_1, \min(\Delta_2, \Delta_3, \Delta_4), \Delta_5, \min(\Delta_6, \Delta_7))$ for the seven-component system. Illustratively, for a scenario where $q_{r,2} \geq \max(q_{r,3}, q_{r,4})$, and $q_{r,7} \geq q_{r,6}$, a working link between A and B is shown in Figure 5B, which can be treated as a series system. In this case, the resource allocation is determined by Equation (30), ignoring the components 3, 4, and 6. Subsequently, a sample value of system resilience, conditional on $q_{r,1}, q_{r,2}, ..., q_{r,7}$, is computed based on Equation (22) or (23). This paves the way for employing the Monte Carlo simulation method to generate nonresilience function.

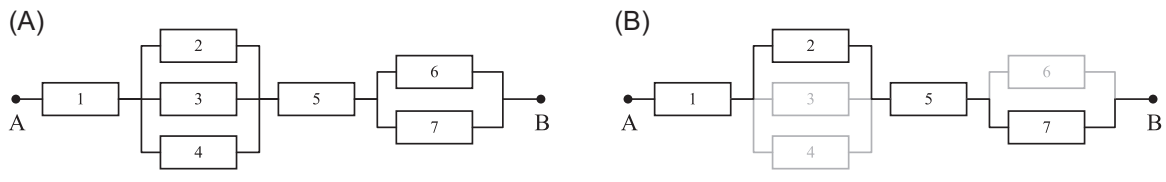

FIGURE 5 A system that links points A and B. (A) A seven-component system, and (B) a working link between points A and B.

The discussions in this section can be extended to other types of general systems (consisting of n components), where the modeling of the recovery process plays a vital role in resilience evaluation. The system recovery duration, Δ_{sys}, is a function of each Δ_i (the recovery duration of the ith component), denoted by $\Delta_{sys} = g(\Delta_1, \Delta_2, ..., \Delta_n)$. With this, the optimal resource allocation strategy can be determined by solving the following:

$$\begin{aligned} &\min_{\mathcal{R}_1, \mathcal{R}_2, ..., \mathcal{R}_n} g(\zeta_1(\mathcal{R}_1, q_{r,1}), \zeta_2(\mathcal{R}_2, q_{r,2}), ..., \zeta_n(\mathcal{R}_n, q_{r,n})) \\ &\text{s.t.} \sum_{i=1}^{n} \mathcal{R}_i = \mathcal{R} \\ &\mathcal{R}_i \geq 0, \quad \forall i = 1, 2, ..., n \end{aligned} \tag{26}$$

Recall that Equations (21) and (25) provide solutions to specific cases of (26).

6 | EXAMPLES

In this section, numerical examples are presented to demonstrate the applicability of the proposed nonresilience curves associated with an individual structure, a series system, a parallel system, and a general system.

6.1 | An individual structure

In this section, an example, as adopted from Wang and Ayyub[37] with modification, is presented to demonstrate the applicability of Equation (7). Consider a multispan continuous steel bridge, which is located in the Central and Southeastern United States (CSUS), and is subjected to seismic hazards. In the aftermath of an earthquake event, the bridge may suffer from one of the following five DSs: none, slight, moderate, extensive, and collapse. Corresponding to each of the DSs, the posthazard remaining functionality (Q_r, written in the capital as it is a random variable) and the fragility curves are presented in Table 1. Suppose that Q_r follows a Beta distribution with a coefficient of variation of 0.2, which has a support of $[0, 1]$ and thus is consistent with the physics of remaining functionality. The fragility curves are conditional on the peak ground acceleration (PGA) with a unit of g (gravitational acceleration). In terms of the recovery process, conditional on $Q_r = q_r > 0$, $\Delta = \zeta(\mathcal{R}, q_r) = (1 - q_r)/\mathcal{R}$ in year. For example, with unit resource ($\mathcal{R} = 1$), it takes 6 months to recover 50% functionality to full performance. However, if $Q_r = 0$ (i.e., the structure fully collapses), assume that there is no subsequent recovery process (i.e., $\zeta(\mathcal{R}, 0) = \infty$). Note that some probability distributions (e.g., that for Q_r) have been assumed in this example for illustration purpose; they may be replaced in practical applications by other types of probability models that are supported and validated by real-world data.

With the above configuration, one can find Ω_1 and Ω_2 (in Equations 9 and 10) as follows:

$$\Omega_1 = \max(0, 1 - \mathcal{R}\Delta_d), 1], \quad \Omega_2 = [0, \max(0, 1 - \mathcal{R}\Delta_d)] \tag{27}$$

Figure 6 shows the nonresilience curves for the bridge associated with a unit resource ($\mathcal{R} = 1$) and two generating functions ($f_1(x)$ and $f_2(x)$, respectively). A reference period of 1 year ($\Delta_{ref} = 1$) is considered with $\Delta_f = 0.01$. For

TABLE 1 Functionality loss and fragility curve of an MSC bridge.

		Seismic fragility curve	
Damage state	**Mean value of Q_r (%)**	**Median PGA (g)**	**Dispersion**
No damage	100	–	–
Slight damage	75	0.18	0.55
Moderate damage	50	0.31	0.55
Extensive damage	25	0.39	0.55
Collapse	0	0.50	0.55

Abbreviations: MSC, multispan continuous; PGA, peak ground acceleration.

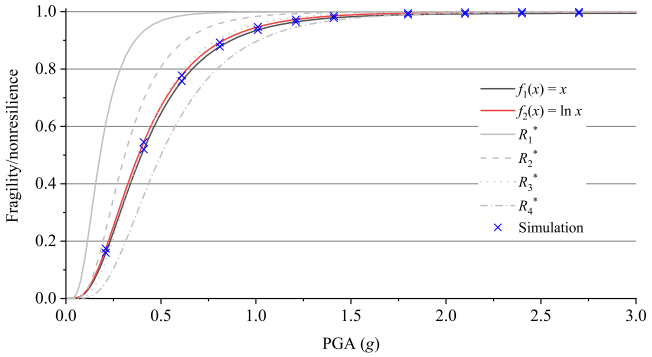

FIGURE 6 Fragility and nonresilience curves of a bridge. PGA, peak ground acceleration.

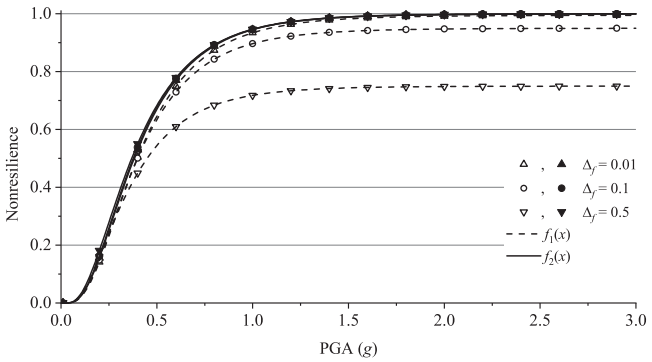

FIGURE 7 Impact of Δ_f on nonresilience curve. PGA, peak ground acceleration.

comparison purpose, the four fragility curves (i.e., CDFs of R_1^*, R_2^*, R_3^*, and R_4^*) are also plotted in Figure 6. The nonresilience curves display a monotonically increasing trend with IM (PGA in this example), due to the increasing seismic risks. The nonresilience obtained with $f_1(x)$ is smaller than that associated with $f_2(x)$, which is consistent with the observation from Wang.[17] The accuracy of the two nonresilience curves in Figure 6 is verified through employing Monte Carlo simulation. The simulated nonresilience (see the legend "×") is obtained by taking the average of sampled nonresiliences (i.e., $1 - R_e$ in Equation 2) for each IM, and is found to agree well with the analytical solution.

In Figure 6, as the $PGA \to \infty$, all the fragility curves and the nonresilience curve associated with $f_2(x)$ approaches 1, implying that the bridge will collapse/become nonresilient in the presence of a sufficiently large IM. However, the nonresilience curve associated with $f_1(x)$ converges to a limit that is smaller than 1 and is impacted by Δ_f. To better demonstrate this point, the effect of Δ_f on the nonresilience curve is examined in Figure 7 with $\mathcal{R} = 1$ and $\Delta_{\text{ref}} = 1$. With a greater value of Δ_f, the limit for $f_1(x)$-related nonresilience curve becomes smaller. This is explained by the resilience model in Equation (9). With a remaining functionality being $q \to 0$, it follows that

$$\overline{R}_{e,j} \to \frac{\Delta_f}{2\Delta_{\text{ref}}} \tag{28}$$

which yields the limit of $\mathcal{N}(x)$ being a function of Δ_f. For example, if $\Delta_f = 0.5$ (see Figure 7), then the $f_1(x)$-related nonresilience curve converges to $1 - 0.5/(2 \times 1) = 0.75$. On the other hand, if the generating function is $f_2(x)$, with Equation (10), $\overline{R}_{e,j} \to 0$. It is a natural assumption that the nonresilience curve approaches 1 with a sufficiently large IM (which is similar to the fragility curves) since the object is nonresilient due to the lack of resource that supports recovery. With this regard, the comparison in Figure 7 demonstrates that the resilience model in Equation (2) with a generating function of $f_2(x)$ is more reasonable compared with that associated with $f_1(x)$.

Note that in Figures 6 and 7, the nonresilience curve is associated with a unit resource. With the IM (PGA) and resource varying simultaneously, one can extend the nonresilience curve to nonresilience surface as a joint function of IM and $\mathcal{R}$. Illustratively, Figure 8 shows the nonresilience curve for the bridge with $\Delta_{\text{ref}} = 1$, $\Delta_f = 0.01$, and $f_2(x)$. The dependence of the nonresilience surface, denoted by $\mathcal{N}(x, \mathcal{R})$, on IM and resource is simultaneously reflected. The

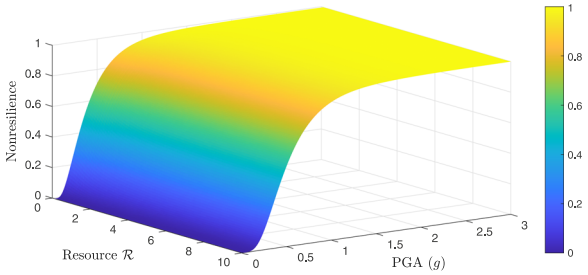

FIGURE 8 Nonresilience surface $\mathcal{N}(x, \mathcal{R})$ as a joint function of PGA and resource $\mathcal{R}$. PGA, peak ground acceleration.

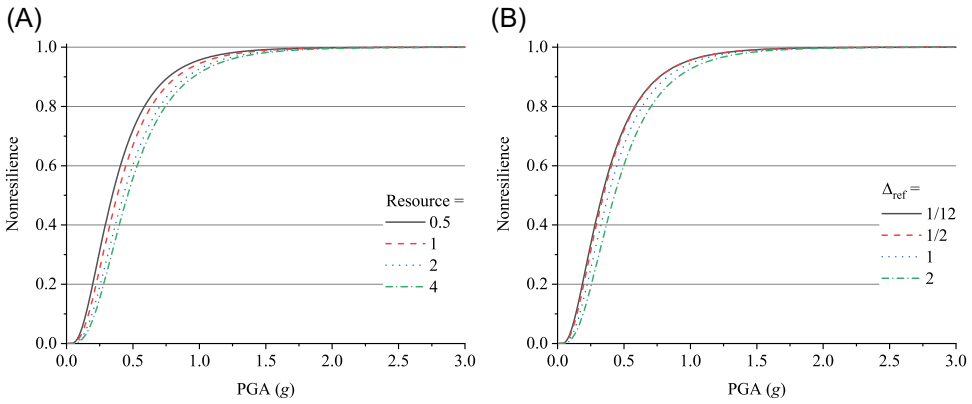

FIGURE 9 Impact of resource and Δ_{ref} on nonresilience curve. (A) Impact of $\mathcal{R}$, and (B) impact of Δ_{ref}. PGA, peak ground acceleration.

cross-section of the nonresilience surface at a specific value of $\mathcal{R}$ yields the nonresilience curve. In particular, the cross-sections of the nonresilience surface at $\mathcal{R} = 0.5$, 1, 2, and 4 are shown in Figure 9A to demonstrate the impact of resource on the nonresilience curve. A greater value of $\mathcal{R}$ results in smaller nonresilience due to the relatively more expeditious recovery process. For instance, with $PGA = 0.5g$, the nonresilience equals 0.721, 0.670, 0.603, and 0.558, respectively, corresponding to $\mathcal{R} = 0.5$, 1, 2, and 4. Furthermore, the impact of Δ_{ref} on the nonresilience curve is shown in Figure 9B, considering unit resource and $f_2(x)$. With a longer reference period of interest (i.e., greater value of Δ_{ref}), the nonresilience becomes smaller, because of the greater probability that the recovery process is completed before t_h.

Recall that the fragility curves are often assumed to have a lognormal distribution shape. This is in particular useful when only limited data points associated with the fragility curves are available, as one can find the approximate fragility curve through fitting the available scatters. Similarly, in the context of nonresilience curve, a natural question is: can we also assume a lognormal distribution shape in the presence of limited data? To investigate this issue, the nonresilience curve in Figure 6 associated with $f_2(x)$ is reexamined as an example. Supposing that only the data points at 0.2, 0.4, ..., 2.8, 3.0 (with a step size of 0.2 and a unit of g) are known, the strong linearity between $\ln x$ and $\Phi^{-1}[\mathcal{N}(x)]$ is observed (where $\Phi()$ is the CDF of a standard normal distribution, and Φ^{-1} is the inverse function of Φ), as plotted in Figure 10A. (Note that the legend "Real data" refers to the scattered data from Figure 6.) Subsequently, the comparison between the real and lognormal distribution-based nonresilience curves is shown in Figure 10B. It can be seen that a lognormal distribution shape can well model the overall trend of the real nonresilience curve, with an R^2 value being >0.999 in Figure 10A.

With the nonresilience function $\mathcal{N}(x)$, one can further evaluate the nonresilience of the bridge in a fully probabilistic manner by taking into account the uncertainty associated with the IM (PGA), as revealed in Equation (4) or (14). This reflects the advantage of employing the proposed nonresilience curve in efficient resilience assessment. To demonstrate this point, the seismic hazard scenarios for two CSUS locations are selected for the bridge, namely, St. Louis, Missouri and Memphis, Tennessee, respectively. The annual maximum PGA, S_a, is modeled by an Extreme Type II distribution, with which the CDF of S_a, $F_{S_a}(x)$, is as follows:

$$F_{S_a}(x) = \exp\left(-\epsilon_a^k x^{-k}\right), \quad x > 0 \tag{29}$$

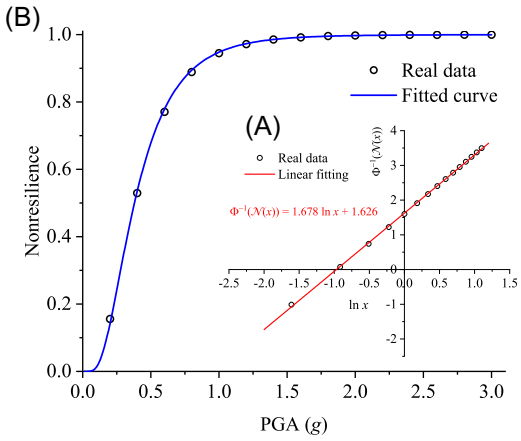

FIGURE 10 Lognormal distribution-based fitting of nonresilience curve. PGA, peak ground acceleration. (A) PGA-Nonresilience relationship in a $\ln x - \Phi^{-1}(y)$, and (B) PGA-Nonresilience relationship.

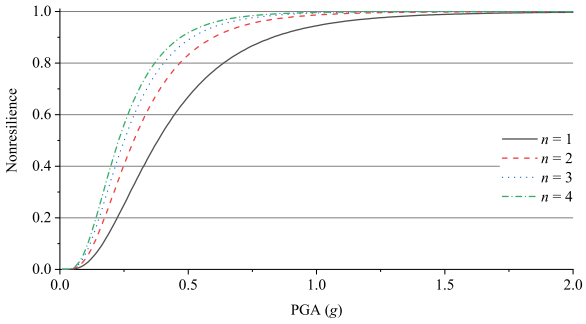

FIGURE 11 Nonresilience curve of a series system consisting of n components. PGA, peak ground acceleration.

in which ϵ_a and k are the scale parameter and shape parameter, respectively. Wang and Teh[38] examined the seismic hazard curves available at the United States Geological Survey, and calibrated the distribution of S_a as follows: for St. Louis, $k = 1.617$, $\epsilon_a = 1.98 \times 10^{-3}$, and for Memphis, $k = 1.409$, $\epsilon_a = 2.28 \times 10^{-3}$.

On the basis of Equation (14), using the nonresilience curve in Figure 6 associated with $f_2(x)$, the nonresilience of the bridge due to S_a equals 3.5×10^{-4} if it is located at St. Louis, and 1.09×10^{-3} if located at Memphis. On the other hand, if using the fitted nonresilience curve obtained in Figure 10, the nonresilience equals 3.2×10^{-4} and 1.01×10^{-3}, respectively, for the two locations. Correspondingly, the error in nonresilience due to the use of fitted nonresilience curve is 8.57% and 7.34%, implying again the appropriateness of assuming a lognormal distribution shape for the nonresilience curve.

6.2 | A series system

Herein, an example is presented to demonstrate the applicability of the nonresilience curve for series systems. Assume that the system consists of n components, and the statistics (including those associated with the fragility curves and remaining functionality) of each component are as in Table 1. Unless otherwise stated, assume that the correlation coefficient between any pair $R^*_{i,1}$ and $R^*_{j,1}$ $(i \neq j)$, denoted by ρ, equals 0.5. A reference period of 1 year after the hazard occurrence is considered (i.e., $\Delta_{\text{ref}} = 1$), with $\Delta_{\text{f}} = 0.01$. The recovery duration of the ith component is modeled as $\zeta_i(\mathcal{R}_i) = (1 - q_{r,i})/\mathcal{R}_i$ for $i = 1, 2, ..., n$. According to Equation (21), $\mathcal{R}_i = (1 - q_{r,i})/x_0$, with which

$$\Delta_{\text{sys}} = x_0 = \frac{n - \sum_{i=1}^{n} q_{r,i}}{\mathcal{R}}, \quad \mathcal{R}_i = \frac{(1 - q_{r,i})\mathcal{R}}{n - \sum_{i=1}^{n} q_{r,i}} \tag{30}$$

Equation (30) implies the impact of n on the posthazard resource allocation strategy, which further affects the system resilience. To demonstrate this point, Figure 11 shows the dependence of system nonresilience on the number

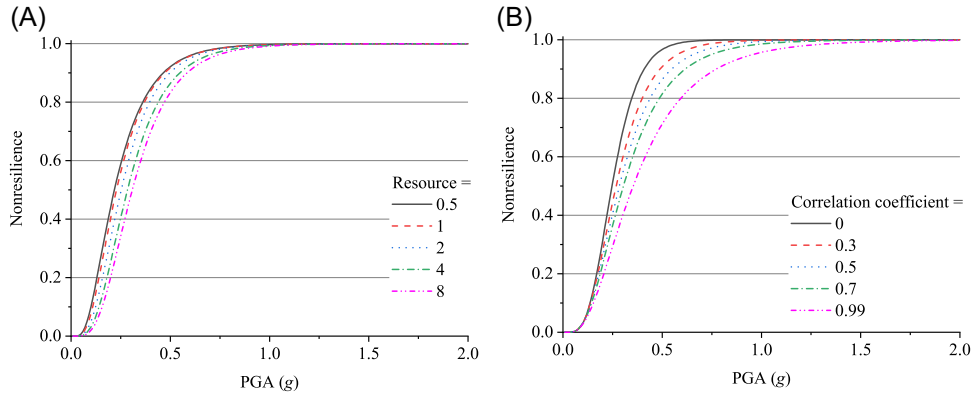

FIGURE 12 Impact of $\mathcal{R}$ and ρ on the nonresilience curve of a four-component series system. (A) Impact of $\mathcal{R}$, and (B) impact of ρ. PGA, peak ground acceleration.

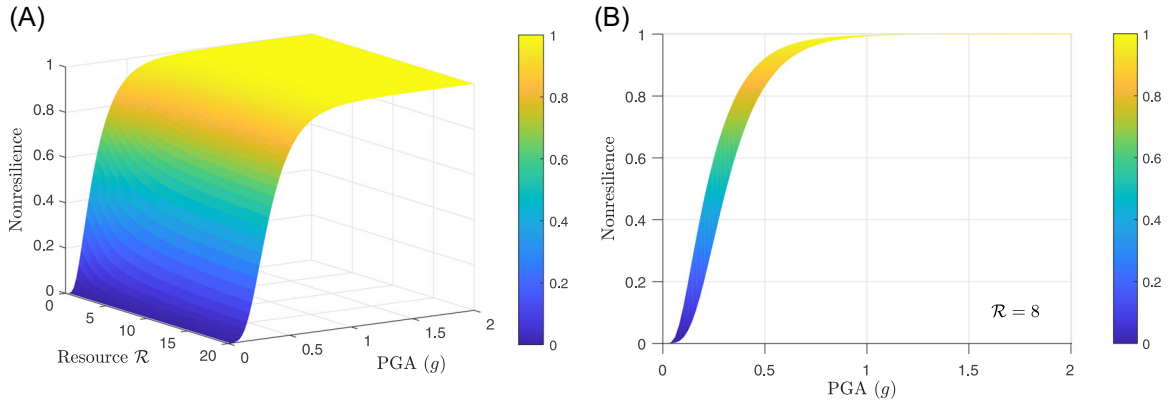

FIGURE 13 Nonresilience surface of a four-component series system. (A) Nonresilience surface, and (B) side view at $\mathcal{R} = 8$. PGA, peak ground acceleration.

of components in the presence of unit resource ($\mathcal{R} = 1$). A larger number of components results in smaller resilience. For example, when $PGA = 0.5g$, the nonresilience equals 0.670, 0.832, 0.890, and 0.918, respectively, corresponding to $n = 1, 2, 3$, and 4. When $n = 1$, the system nonresilience curve degrades to that of an individual structure (component) in Figure 6.

The impact of total resource, $\mathcal{R}$, on the system nonresilience is shown in Figure 12A with $n = 4$. A greater value of $\mathcal{R}$ enables shortened recovery duration (note that each Δ_i is proportional to $1/\mathcal{R}_i$ in this example), and thus results in smaller nonresilience. In Figure 12B, the role of correlation between the generalized capacities of different components is examined with $n = 4$ and $\mathcal{R} = 4$. A greater value of ρ leads to smaller nonresilience. This is because, more weakly correlated component capacities mean the behaviors of these components are less synchronous, with which the occurrence probability of the weakest component with low remaining functionality is amplified.

Similar to the nonresilience surface in Figure 8, one can also extend the system nonresilience curve to nonresilience surface, by additionally considering the variation of resource $\mathcal{R}$. Figure 13A shows the nonresilience surface of a four-component series system, where both the IM (PGA) and $\mathcal{R}$ vary. The cross-section of nonresilience surface, by fixing one of the independent variables, degrades to nonresilience curve. For instance, if making a cut at $\mathcal{R} = 8$, the side view of the nonresilience surface is shown in Figure 13B. The two edges yield the nonresilience curves associated with $\mathcal{R} = 0$ and 8, respectively.

6.3 | A parallel system

This section presents an example on the nonresilience curve of a parallel system with n components. The recovery duration is modeled as $\zeta_i(\mathcal{R}_i) = (1 - q_{r,i})/\mathcal{R}_i$ for each component, with which $\Delta_{\text{sys}} = (1 - q_{\text{sys}})/\mathcal{R}$. Using the same

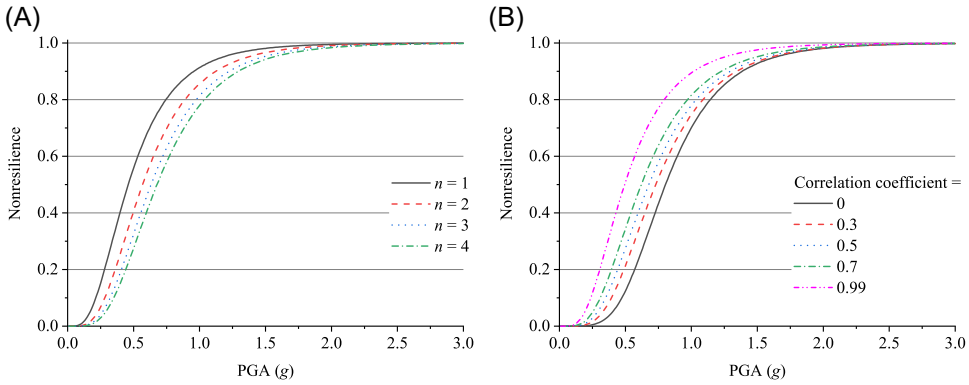

FIGURE 14 Nonresilience curve of a parallel system affected by the number of components and component capacity correlation. (A) Impact of n, and (B) impact of ρ. PGA, peak ground acceleration.

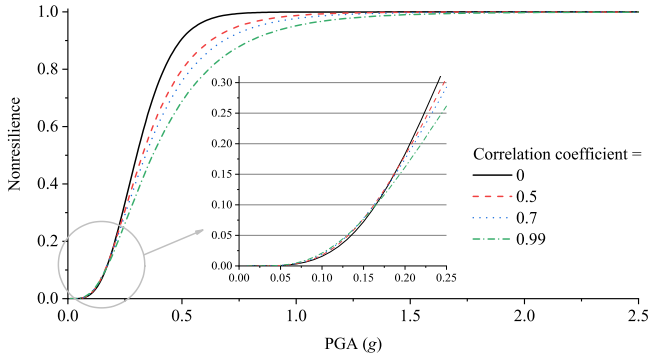

FIGURE 15 Nonresilience curve of the seven-component general system in Figure 5A. PGA, peak ground acceleration.

configuration as in Figure 11 but with $\mathcal{R} = 4$, the nonresilience curve for the parallel system is shown in Figure 14A considering different numbers of components. A greater value of n results in smaller nonresilience, which is different from the observation in Figure 11. This is because the system functionality is determined by the maximum functionality associated with the components of a parallel system. The case of $n = 1$ reduces to the nonresilience curve of a single component as in Figure 6 (see the curve associated with $f_2(x)$). In Figure 14B, the impact of ρ (correlation between the generalized capacities of different components) on the system nonresilience curve is investigated. A greater value of ρ means that the performances of the components are more significantly synchronized, which has a similar effect of reduced number of components on resilience. This thus leads to greater nonresilience, as observed in Figure 14B. The findings from Figure 14 are different from those from Figures 11 and 12B, due to the difference in the definitions of series and parallel systems (with a focus on the minimum and maximum of the component functionalities, respectively).

6.4 | A general system

Using the same configuration as in Figure 12B for the components, the nonresilience curves of the seven-component general system (as shown in Figure 5) with different values of ρ (component capacity correlation) are presented in Figure 15. The emphasis herein is to examine the dependence of system resilience on the topological structure. With a large PGA (e.g., ≥0.2g), a larger value of ρ results in smaller nonresilience, which is similar to the behavior of a series system (see Figure 1B2). However, this effect is reversed in the presence of a small PGA, which is similar to the case of a parallel system in Figure 14B.

The nonresilience curves of systems can also be used to compute the nonresilience of the system in a fully probabilistic manner based on Equation (14). Illustratively, consider the following three system nonresilience curves:

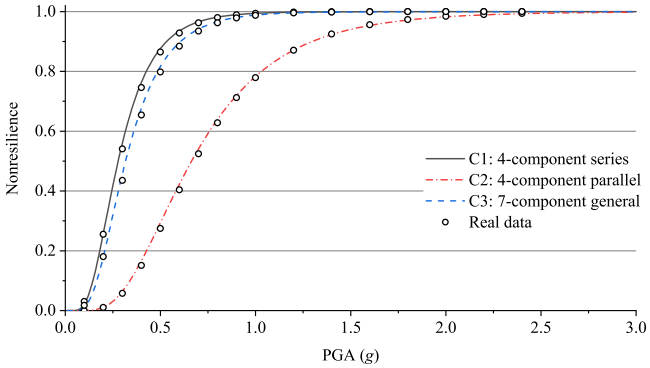

FIGURE 16 Lognormal distribution-based fitting of system nonresilience curves. PGA, peak ground acceleration.

(C1) the curve from Figure 12A with $n = 4$ and $\mathcal{R} = 4$ (series system), (C2) the curve from Figure 14A with $n = 4$ and $\mathcal{R} = 4$ (parallel system), and (C3) the curve from Figure 5 with $n = 7$ and $\mathcal{R} = 4$ (general system). Due to the annual maximum PGA as in Equation (29), if the system is located at St. Louis, the nonresilience equals 4.84×10^{-4}, 1.07×10^{-4}, and 3.84×10^{-4} corresponding to the three nonresilience curves. However, if the system is at Memphis, then the nonresilience becomes 1.48×10^{-3}, 3.90×10^{-4}, and 1.21×10^{-3}, respectively. In particular, the nonresilience associated with the seven-component system is smaller than that of the four-component series system, because the former can be treated as a four-component series system (by grouping components (2, 3, 4) and (6, 7), respectively, as two virtual components) with greater redundancy.

Recall that in Figure 10, the lognormal distribution shape has been tested for the nonresilience curve associated with an individual component. Similarly, one may ask: is the lognormal distribution shape also applicable for system nonresilience curves? To investigate this point, assume that only limited data points associated with the three system nonresilience curves, C1, C2, and C3, are available at $PGA = 0.1, 0.2, ..., 1, 1.2, 1.4, ..., 2.4$ with a unit of g. On the basis of these scatters, the fitted nonresilience curves based on a lognormal distribution shape are shown in Figure 16. The real and fitted curves agree well with each other, implying that a lognormal distribution is also suitable to model the overall shape of the system nonresilience curves.

If the system is located at St. Louis, the system nonresilience due to S_a equals 4.65×10^{-4}, 1.11×10^{-4}, and 3.73×10^{-4}, respectively, using the fitted nonresilience curves for C1, C2, and C3, respectively. This corresponds to an error in nonresilience of -3.82%, 3.46%, and -2.94% compared with the real data-based nonresilience. However, considering the seismic hazard in Memphis, the system nonresilience based on the fitted nonresilience curves equals 1.45×10^{-3}, 4.03×10^{-4}, and 1.19×10^{-3} respectively, introducing an error in nonresilience of -2.57%, 3.16%, and -1.76%.

7 | CONCLUSIONS

In this paper, a novel concept of nonresilience curve has been proposed to measure the nonresilience of an object (an individual structure or a system) conditional on a specific hazard IM. The nonresilience curve is essentially connected with the fragility curves as it integrates the multiple DSs of a posthazard object. The nonresilience curve can be further extended to nonresilience surface by additionally considering the variation of the available resource (as the second independent variable). The following conclusions can be made from this paper.

1. Since the nonresilience curve is conditional on a specific IM, one can further evaluate the nonresilience of an object in a fully probabilistic manner by considering the probability distribution of the IM, based on the total law of total probability.
2. For a posthazard series system, the optimal resource allocation strategy is to ensure that each damaged component is fully restored with the same recovery duration. However, for a parallel system, the optimal strategy is to invest all the resource to the component with the least damage.
3. The system nonresilience is dependent on the system topology, reference period of interest, correlation between components and available resource. In particular, a stronger correlation between components results in smaller nonresilience for series systems, but greater nonresilience for parallel systems.

4. It has been preliminarily shown that, for cases where limited data points associated with the nonresilience curve are available, one can use the CDF of a lognormal distribution to approximate the overall shape of the nonresilience curve. It is an interesting topic in future works to check the generality of the lognormal distribution shape for nonresilience curves.

Finally, it is noted that the nonresilience curve in this paper has been developed based on the probabilistic models of random variables. For the cases where imprecise probabilistic information is involved,[39,40] the nonresilience curve cannot be uniquely determined but varies within an interval, which is worthy of future research works.

ACKNOWLEDGMENTS

The research described in this paper was supported by the Vice-Chancellor's Postdoctoral Research Fellowship and the Career Development Fellowship from the University of Wollongong. These supports are gratefully acknowledged. The author would like to acknowledge the thoughtful suggestions of three anonymous reviewers, which substantially improved the present paper. Open access publishing facilitated by University of Wollongong, as part of the Wiley - University of Wollongong agreement via the Council of Australian University Librarians.

CONFLICTS OF INTEREST

The authors declare no conflicts of interest.

DATA AVAILABILITY STATEMENT

The data that support the findings of this study are available from the author upon reasonable request.

ORCID

Cao Wang http://orcid.org/0000-0002-2802-1394

REFERENCES

1. Bruneau M, Chang SE, Eguchi RT, et al. A framework to quantitatively assess and enhance the seismic resilience of communities. *Earthquake Spectra*. 2003;19(4):733-752.
2. Singh RR, Bruneau M, Stavridis A, Sett K. Resilience deficit index for quantification of resilience. *Resilient Cities Struct*. 2022;1(2):1-9.
3. National Research Council. *Disaster Resilience: A National Imperative*. The National Academies Press; 2012.
4. McAllister T. *Developing Guidelines and Standards for Disaster Resilience of the Built Environment: A Research Needs Assessment*. US Department of Commerce, National Institute of Standards and Technology; 2013.
5. Ayyub BM. Systems resilience for multihazard environments: definition, metrics, and valuation for decision making. *Risk Anal*. 2014;34(2):340-355.
6. Cimellaro GP, Reinhorn AM, Bruneau M. Framework for analytical quantification of disaster resilience. *Eng Struct*. 2010;32(11):3639-3649.
7. Bocchini P, Frangopol DM, Ummenhofer T, Zinke T. Resilience and sustainability of civil infrastructure: toward a unified approach. *J Infrastruct Syst*. 2014;20(2):04014004.
8. Hosseini S, Barker K, Ramirez-Marquez JE. A review of definitions and measures of system resilience. *Reliability Eng Syst Saf*. 2016;145:47-61.
9. Attoh-Okine NO, Cooper AT, Mensah SA. Formulation of resilience index of urban infrastructure using belief functions. *IEEE Syst J*. 2009;3(2):147-153.
10. Salem S, Campidelli M, El-Dakhakhni WW, Tait MJ. Resilience-based design of urban centres: application to blast risk assessment. *Sustainable Resilient Infrastruct*. 2018;3(2):68-85.
11. Sun W, Bocchini P, Davison BD. Resilience metrics and measurement methods for transportation infrastructure: the state of the art. *Sustainable Resilient Infrastruct*. 2020;5(3):168-199.
12. Huang Z, Zhang D, Pitilakis K, et al. Resilience assessment of tunnels: framework and application for tunnels in alluvial deposits exposed to seismic hazard. *Soil Dyn Earthquake Eng*. 2022;162:107456.
13. Shang Q, Wang T, Li J. A quantitative framework to evaluate the seismic resilience of hospital systems. *J Earthquake Eng*. 2022;26(7):3364-3388.
14. Pang Y, Wei K, He H, Wang W. Assessment of lifetime seismic resilience of a long-span cable-stayed bridge exposed to structural corrosion. *Soil Dyn Earthquake Eng*. 2022;157(4):107275.
15. Capacci L, Biondini F, Frangopol DM. Resilience of aging structures and infrastructure systems with emphasis on seismic resilience of bridges and road networks. *Resilient Cities Struct*. 2022;1(2):23-41.
16. Du A, Wang X, Xie Y, Dong Y. Regional seismic risk and resilience assessment: methodological development, applicability, and future research needs—an earthquake engineering perspective. *Reliability Eng Syst Saf*. 2023;223:109104.

17. Wang C. A generalized index for functionality-sensitive resilience quantification. *Resilient Cities Struct*. 2023;2(1):68-75.
18. Li Y, Ellingwood BR. Hurricane damage to residential construction in the US: importance of uncertainty modeling in risk assessment. *Eng Struct*. 2006;28(7):1009-1018.
19. Kirçil MS, Polat Z. Fragility analysis of mid-rise R/C frame buildings. *Eng Struct*. 2006;28(9):1335-1345.
20. Choe DE, Gardoni P, Rosowsky D, Haukaas T. Probabilistic capacity models and seismic fragility estimates for RC columns subject to corrosion. *Reliability Eng Syst Saf*. 2008;93(3):383-393.
21. Ghosh J, Padgett JE. Aging considerations in the development of time-dependent seismic fragility curves. *J Struct Eng*. 2010;136(12):1497-1511.
22. Shinozuka M, Feng MQ, Lee J, Naganuma T. Statistical analysis of fragility curves. *J Eng Mech*. 2000;126(12):1224-1231.
23. Baker JW. Introducing correlation among fragility functions for multiple components. In: *Proceedings of the 14th World Conference on Earthquake Engineering, Beijing, China, October 12–17, 2008*; 2008.
24. Wang C, Zhang H, Ellingwood BR, Guo Y, Mahmoud H, Li Q. Assessing post-hazard damage costs to a community's residential buildings exposed to tropical cyclones. *Struct Infrastruct Eng*. 2020;17(4):443-453.
25. Wang C, Zhang H. Assessing the seismic resilience of power grid systems considering the component deterioration and correlation. *ASCE-ASME J Risk Uncertainty Eng Syst Part B*. 2020;6(2):020903.
26. Shiraki N, Shinozuka M, Moore JE, Chang SE, Kameda H, Tanaka S. System risk curves: probabilistic performance scenarios for highway networks subject to earthquake damage. *J Infrastruct Syst*. 2007;13(1):43-54.
27. FEMA. *Multi-hazard Loss Estimation Methodology, Earthquake Model: Hazus-MH 2.1*. Department of Homeland Security, Federal Emergency Management Agency, Mitigation Division; 2012.
28. Wang C, Ayyub BM, Beer M. From reliability-based design to resilience-based design. *ASCE-ASME J Risk Uncertainty Eng Syst Part B*. 2023;9(3):031105.
29. Panteli M, Mancarella P. Modeling and evaluating the resilience of critical electrical power infrastructure to extreme weather events. *IEEE Syst J*. 2015;11(3):1733-1742.
30. Poulin C, Kane MB. Infrastructure resilience curves: performance measures and summary metrics. *Reliability Eng Syst Saf*. 2021;216:107926.
31. Ayyub BM. Practical resilience metrics for planning, design, and decision making. *ASCE-ASME J Risk Uncertainty Eng Syst Part A*. 2015;1(3):04015008.
32. Ross SM. *Introduction to Probability and Statistics for Engineers and Scientists*. Academic Press; 2020.
33. Vitoontus S. *Risk Assessment of Building Inventories Exposed to Large Scale Natural Hazards*. Ph.D. Thesis. Georgia Institute of Technology; 2012.
34. Liu PL, DerKiureghian A. Multivariate distribution models with prescribed marginals and covariances. *Probab Eng Mech*. 1986;1(2 105-112.
35. Melchers RE, Beck AT. *Structural Reliability Analysis and Prediction*. John Wiley & Sons; 2018.
36. Wang C. *Structural Reliability and Time-Dependent Reliability*. Springer Nature; 2021.
37. Wang C, Ayyub BM. Time-dependent seismic resilience of aging repairable structures considering multiple damage states. *Earthquake Eng Resilience*. 2022;1(1):73-87.
38. Wang C, Teh LH. Time-dependent seismic reliability of aging structures. *ASCE-ASME J Risk Uncertainty Eng Syst Part A*. 2022;8(2):04022010.
39. Wang C, Zhang H, Beer M. Computing tight bounds of structural reliability under imprecise probabilistic information. *Comput Struct*. 2018;208:92-104.
40. Faes MG, Daub M, Marelli S, Patelli E, Beer M. Engineering analysis with probability boxes: a review on computational methods. *Struct Saf*. 2021;93:102092.

How to cite this article: Wang C. Nonresilience curve: a new tool for use in resilience assessment. *Earthq Eng Resil*. 2024;3:54-71. doi:10.1002/eer2.73